A smeared crack formulation for simulating fracture of fibre-reinforced concrete by means of a trilinear softening diagram

F. Suárez[a]

[a]*Departamento de Ingeniería Mecánica y Minera. Universidad de Jaén. Campus Científico-Tecnológico de Linares. Cinturón Sur 23700-Linares (Jaén)*

Abstract

In this study, a material model is proposed for reproducing the fracture behaviour of FRC. Unlike previous models, developed for commercial codes, this model is developed in OOFEM, a free finite element code developed at the Czech Technical University in Prague (Czech Republic) and Chalmers University of Technology (Sweden), thus providing the general public with a tool that allows reproducing fracture in structural elements made with fibre-reinforced concrete elements. The model proposed in this work differs from the one on which it is inspired, since it is a smeared crack model based on the crack band concept where the material damage is isotropic and controlled by a damage factor ranging from 0 to 1, while the original model is an embedded crack model that allows fracture in three directions per element. This formulation overcomes some limitations of the model of reference, that could only be used with triangular elements with an only integration point, sine it can be used with triangular and quadrilateral elements with any number of integration points. This work shows that the proposed formulation provides similar results to those obtained with the model on which it is inspired under different situations: mode I fracture, size effect analysis and, finally, modes I and II mixed fracture.

Keywords: Fibre-reinforced concrete, Trilinear softening function, OOFEM, Cohesive model, Smeared crack.

1. Introduction

In recent times, fibre-reinforced concrete (FRC) has aroused increasing interest in construction, which has boosted the appearance of new fibres onto the market and the recommendations for their use that are included in several structural standards around the world [1, 2, 3, 4]. The use of fibres as reinforcement of concrete cannot be considered as a new technique, since it has been used in certain tasks for decades, such as tunnel lining and floor reinforcement in airports and industrial areas [5, 6]. Nevertheless, although steel fibres were initially used in FRC, there are now a wide variety of fibres that can be used as reinforcement, depending on the material properties that need to be modified (see Fig. 1). For example, polypropylene microfibres are used for reducing cracking due to shrinkage [7, 8], glass fibres can be employed as reinforcement in façade panels [9, 10] or in telecommunication towers [11] and recent polymer fibres can provide structural properties to concrete, reducing the amount of steel rebars and even completely removing them [12, 13].

Numerical modeling of the behaviour of these new materials is of great importance, since if their use is to be extended, engineering professionals need to count with reliable models that allow reproducing their behavior in engineering projects. In this sense, fracture of concrete has been extensively studied in the last decades and many models have been proposed to be used within the framework of the finite element analysis, which is the most extended tool for dealing with these problems. Some of these models, discrete models, reproduce fracture when an only crack is formed [14], while others, smeared crack models, modify the material constitutive equations to account for the presence of several cracks in the damaged element that are evenly distributed over the element [15]. There is another interesting type of models, embedded crack

*F. Suárez
Email address: fsuarez@ujaen.es (F. Suárez)

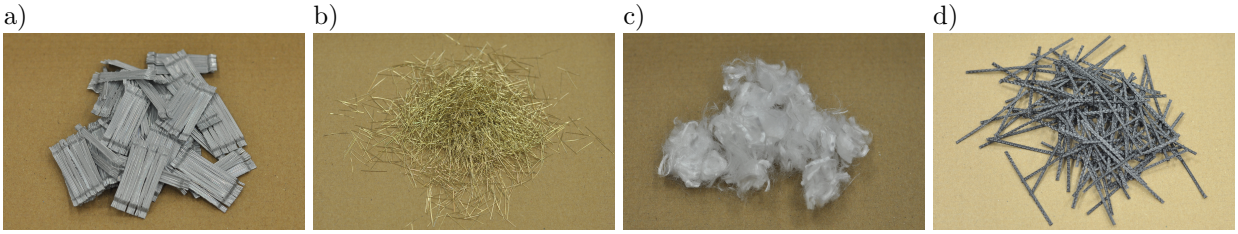

Figure 1: Some fibre types uses as reinforcement in FRC: a) steel macrofibres, b) steel microfibres, c) polypropylene microfibres and d) polyolefin macrofibres.

models, that include the effect of cracking by enriching the displacement or the strain fields in the element formulation [16, 17]. Many reliable formulations for concrete fracture can be found in the literature, often based on the cohesive zone concept, developed by Hillerborg [18], which has proven to be a relatively simple way of reproducing fracture, and has been extended since its appearance and is still very commonly used in Fracture Mechanics.

While many fracture models are available for concrete, not so many can be found for FRC and different approaches can be observed. For example, in the case of the model proposed by Havlásek and Kabele [19], the material behaviour is derived from the material properties of the components, fibres and matrix, while in the case of the model proposed by Alberti et al. [20], the material behaviour is described by a softening diagram that can be obtained experimentally (the parameters that identify the softening diagram can be related to specific values of the matrix and the fibres, although not directly). The latter model has proven to be effective in many situations, such as mode I fracture with different fibre-proportion additions [20], different production processes of the mix and mixed-mode fracture (I+II) [21].

In the present work, a cohesive crack model is proposed for modelling fracture of FRC. This model can be classified as a smeared crack model, where the proper amount of dissipated energy during the fracture process is guaranteed by the crack-band approach [22], with the crack band width given by the size of the finite element projected in the direction of the principal stress, as suggested by Oliver [23]. The model is based on the trilinear diagram proposed by Alberti et al. [20] but, while in that case fracture was modeled by means of an embedded cohesive crack where cohesive stress evolved with crack opening, in the model proposed here fracture is controlled by a damage factor that ranges from 0 (undamaged material) to 1 (completely damaged material). This model is implemented in OOFEM [24], a free finite element code developed at the Czech Technical University in Prague (Czech Republic) and the Chalmers University of Technology (Sweden). This new formulation not only provides anyone interested in the fracture behaviour of FRC a free tool to use, but also overcomes some limitations of the model of reference, which could only be used with triangular elements with an only integration point. The formulation proposed here can be used with any bidimensional element employing any number of integration points and, as the validation of the model will show, it provides a more robust tool for modeling fracture of this type of materials.

Since the model on which this work is inspired has been used and studied widely in the past, it is deemed appropriate to compare the results of the new formulation with those obtained with the embedded formulation proposed by Alberti et al., in order to check if both formulations provide similar results. For this reason, the second section of this work provides a brief description of the embedded crack formulation and the third section presents the smeared crack formulation proposed here. The fourth section corresponds to the validation of the model, that is carried out by reproducing numerical results of polyolefin-fibre reinforced concrete (PFRC), available in the literature, and comparing them with those obtained with the embedded crack model, more especifically: i) mode I fracture of a three-point bending test is reproduced for different fibre proportions, ii) mesh-size influence on the results is analysed, iii) the ability of the model for capturing the size effect of FRC fracture is studied and iv) mixed-mode fracture (I+II) is reproduced.

2. Existing embedded cohesive crack with a trilinear softening diagram

This section briefly describes the main features of the embedded cohesive crack model on which the proposed model, that will be presented later, is based. Note that here only a basic description will be made, referring to those aspects that are relevant to the comparison between both models that will be presented later. The reader can find a more detailed description in [25, 26], which presents the original formulation, valid for concrete, and [20, 21], which adapts it to fibre-reinforced concrete.

2.1. Cohesive crack model

This model is based on the cohesive crack concept by Hillerborg and describes fracture inside a triangular element by means of a strong discontinuity approach. The model is a central forces model, since the cohesive stress vector $\boldsymbol{t}$ is constant along the crack and parallel to the displacement vector $\boldsymbol{w}$ (see Fig. 2) and is computed as shown in expression (1).

$$\boldsymbol{t} = \frac{f\left(\tilde{w}\right)}{\tilde{w}}\boldsymbol{w} \quad \text{with } \tilde{w} = \max|\boldsymbol{w}| \tag{1}$$

This formulation is applied to constant stress triangular elements and only allows fracture in three directions, parallel to each side of the triangle. The stress of the damaged element is computed by subtracting an inelastic part to the elastic behaviour of the element, as shown in expression (2), where $\boldsymbol{E}$ represents the tangent elastic tensor, $\boldsymbol{\epsilon}^a$ the apparent strain vector, $\boldsymbol{b}^+$ gradient vector of the shape function of the solitary node (the one in A^+ in Fig. 2) and can be obtained as $\boldsymbol{b}^+ = \frac{1}{h}\boldsymbol{n}$, superscript S represents the symmetric part of the resulting tensor, : is the usual double-dot product ($(\boldsymbol{A} : \boldsymbol{b})_{ij} = A_{ijkl}b_{kl}$) and $\otimes$ is the direct product ($(\boldsymbol{a} \otimes \boldsymbol{b})_{ij} = a_i b_j$).

$$\boldsymbol{\sigma} = \boldsymbol{E} : \left[\boldsymbol{\epsilon}^a - \left(\boldsymbol{b}^+ \otimes \boldsymbol{w}\right)^S\right] \cdot \boldsymbol{n} \tag{2}$$

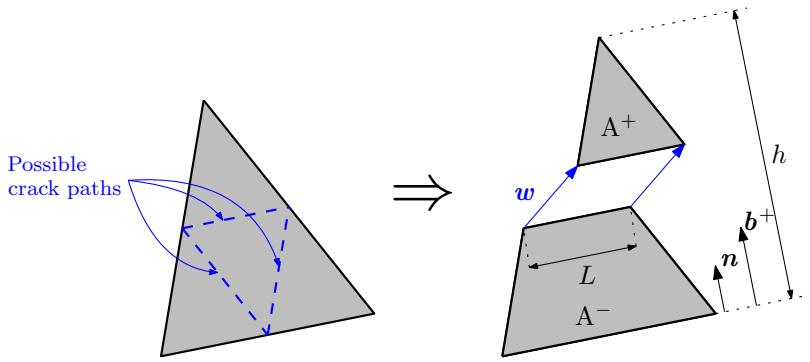

Figure 2: Scheme of the main elements of the embedded cohesive crack model (right) and the possible crack paths (left).

2.2. Trilinear softening diagram

This embedded crack model describes damage as crack progresses by means of a softening diagram, expressed in terms of stress (σ) and crack opening (w). This softening diagram is traditionally described for concrete by linear, bilinear and exponential functions [27], but a trilinear diagram can be used for reproducing the fracture behaviour of FRC, as shown in Fig. 3. This diagram is defined by four points (t, k, r and f), with coordinates that are related to specific characteristics of the FRC mix, such as the fibre proportion, the fibre length or the mechanical properties of the fibre material [20]. Once the six parameters of this diagram are defined (f_t, f_k, f_r, w_k, w_r and w_f), the stress corresponding to a specific crack opening value can be obtained as shown by (3).

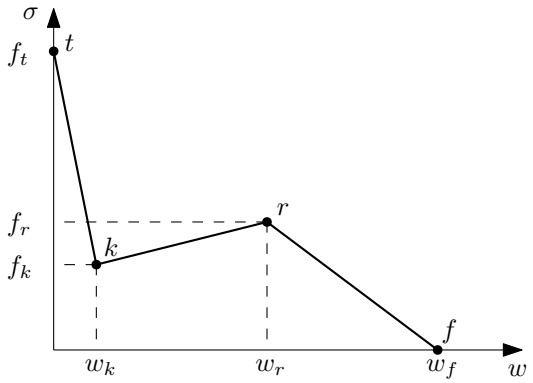

Figure 3: Trilinear softening diagram proposed in [20] for adapting the embedded crack model in [25] to HRF.

$$\sigma = \begin{cases} f_t + \left(\dfrac{f_k - f_t}{w_k}\right) \cdot w & \text{if } 0 < w \leq w_k \\ f_k + \left(\dfrac{f_r - f_k}{w_r - w_k}\right) \cdot (w - w_k) & \text{if } w_k < w \leq w_r \\ f_r + \left(\dfrac{-f_r}{w_f - w_r}\right) \cdot (w - w_r) & \text{if } w_r < w \leq w_f \\ 0 & \text{if } w > w_f \end{cases} \tag{3}$$

3. Proposed smeared crack model with a trilinear softening diagram

The formulation proposed here corresponds to a smeared crack model where damage is isotropic, so that the stiffness tensor of the material $\boldsymbol{D}$ is expressed as:

$$\boldsymbol{D} = (1 - \omega)\, \boldsymbol{D}_e \tag{4}$$

where $\boldsymbol{D}_e$ represents the elastic stiffness tensor and ω is a scalar damage variable [1] ranging from 0 (not damaged material) to 1 (completely damaged material).

Damage evolution takes into account the damage variable ω and also the largest previously reached strain value. For computing the strain state at each step, an equivalent strain value is used, ε_{eq}, which is obtained by means of the strain tensor components. This equivalent strain can be computed using different expressions; here the Rankine criterion, expressed in (5), is employed:

$$\varepsilon_{eq} = \frac{1}{E} \sqrt{\sum_{I=1}^{3} \langle \bar{\sigma}_I \rangle^2} \tag{5}$$

where E stands for the elastic modulus of the matrix, $\bar{\sigma}_I$ represents the principal stresses ($I = 1, 2, 3$), with $\langle \bar{\sigma}_I \rangle$ being only their positive values.

The evolution of damage, which directly influences the material behaviour through expression (4), must be related to the equivalent strain obtained with (5). To do this, the crack band theory proposed by Bažant and Oh [28] is employed, which analyses cracking inside a finite element as a crack opening w through a band of thickness h. The proper amount of dissipated energy is ensured by distributing the crack over an effective thickness h that is estimated by projecting the finite element onto the direction of the maximum principal strain at the onset of damage, as suggested by Oliver [23]. Therefore, the crack opening can be obtained by

[1] Please,note that ω represents damage while w represents crack opening.

$w = \varepsilon_c h$, where the inelastic strain ε_c is the difference between the total strain and the elastic strain (σ/E), as expressed by (6).

$$\varepsilon_c = \varepsilon_{eq} - \frac{\sigma}{E} \tag{6}$$

If the cohesive stress is obtained with the damage parameter through (4), it can be expressed by (7), thus expression (6) results in (8). Therefore, the crack opening can be obtained with (9).

$$\sigma = (1-\omega)E\varepsilon_{eq} \tag{7}$$

$$\varepsilon_c = \varepsilon_{eq} - \frac{(1-\omega)E\varepsilon_{eq}}{E} \Rightarrow \varepsilon_c = \omega\varepsilon_{eq} \tag{8}$$

$$w = h\varepsilon_c = h\omega\varepsilon_c \tag{9}$$

Since one of the main objectives in this work is to compare the results obtained with the proposed formulation with the embedded crack formulation on which it is inspired, the expression of the damage parameter ω is now obtained expressed with the same parameters used in it, which are those that define the trilinear diagram (f_t, f_k, f_r, w_k, w_r and w_f). On the left of Fig. 4 the trilinear diagram expressed in terms of the crack opening, as used in the embedded crack model presented in section 2 is shown, and on the right of the same figure the equivalent diagram expressed in terms of the equivalent strain ε_{eq} can be observed. The expression of ω is obtained for all five possible cases, from undamaged material ($\omega = 0$) up to totally damaged material ($\omega = 1$). First and last cases are trivial so, in what follows, the three intermediate cases are presented. Note that, as shown in Fig. 4, ε_0 identifies the value of the equivalent strain at which damage starts to develop.

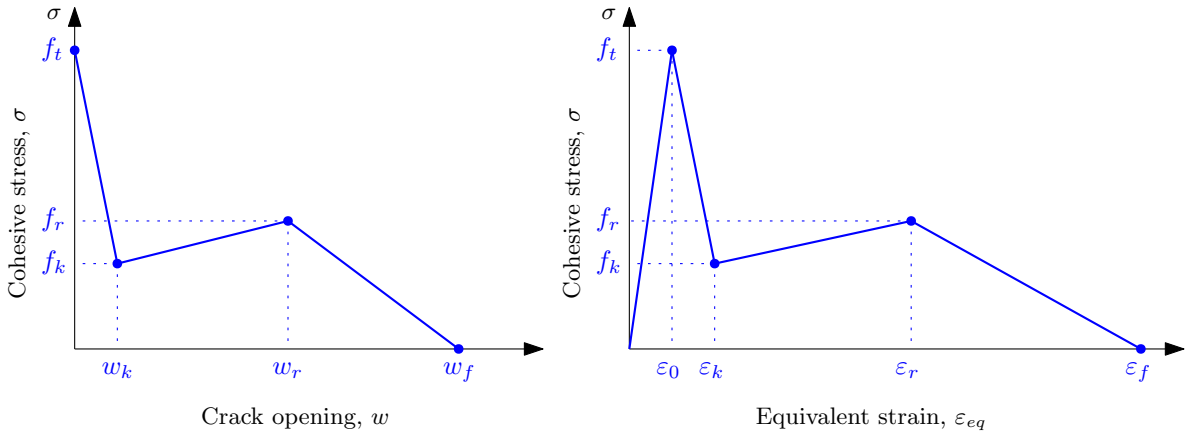

Figure 4: Trilinear diagram expressed in terms of the crack opening w (left) and expressed in terms of the equivalent strain (ε_{eq}).

- **Case 2:** $\varepsilon_0 \leq \varepsilon_{eq} \leq \varepsilon_k$: As shown in (3), cohesive stress in this case is obtained by:

$$\sigma = f_t + \left(\frac{f_k - f_t}{w_k}\right) \cdot w \tag{10}$$

Since, $f_t = E\varepsilon_0$ and substituting expressions (7) and (9) in (10), ω is obtained as follows:

$$(1-\omega)E\varepsilon_{eq} = E\varepsilon_0 + h\omega\varepsilon_{eq}\left(\frac{f_k - f_t}{w_k}\right) \quad \Rightarrow$$

$$\Rightarrow \quad \omega = \frac{E}{E + h\left(\frac{f_k - f_t}{w_k}\right)} - \frac{E\varepsilon_0}{\varepsilon_{eq}\left[E + h\left(\frac{f_k - f_t}{w_k}\right)\right]}$$

- **Case 3:** $\varepsilon_k \leq \varepsilon_{eq} \leq \varepsilon_r$: In this case, as shown in (3), cohesive stress is:

$$f_k + \left(\frac{f_r - f_k}{w_r - w_k}\right) \cdot (w - w_k) \tag{11}$$

Therefore, with expressions (7) and (9), ω can be obtained as follows:

$$(1-\omega)E\varepsilon_{eq} = f_k + (h\omega\varepsilon_{eq} - w_k)\left(\frac{f_r - f_k}{w_r - w_k}\right) \quad \Rightarrow$$

$$\Rightarrow \quad \omega = \frac{E}{E + h\left(\frac{f_r - f_k}{w_r - w_k}\right)} + \frac{1}{\varepsilon_{eq}} \cdot \frac{w_k\left(\frac{f_r - f_k}{w_r - w_k}\right) - f_k}{E + h\left(\frac{f_r - f_k}{w_r - w_k}\right)}$$

- **Case 4:** $\varepsilon_r \leq \varepsilon_{eq} \leq \varepsilon_f$: In this case, as shown in (3), cohesive stress is:

$$f_r + \left(\frac{-f_r}{w_f - w_r}\right) \cdot (w - w_r) \tag{12}$$

Proceeding as in the previous two cases, ω is obtained as follows:

$$(1-\omega)E\varepsilon_{eq} = f_r + (h\omega\varepsilon_{eq} - w_r)\left(\frac{-f_r}{w_f - w_r}\right) \quad \Rightarrow$$

$$\Rightarrow \quad \omega = \frac{E}{E + h\left(\frac{-f_r}{w_f - w_r}\right)} + \frac{1}{\varepsilon_{eq}} \cdot \frac{w_r\left(\frac{-f_r}{w_f - w_r}\right) - f_r}{E + h\left(\frac{-f_r}{w_f - w_r}\right)}$$

These expressions allow feeding the fracture with exactly the same input parameters as in the embedded crack formulation with which it will be compared. This is relevant in order to take advantage of all the knowledge acquired in the past using the model of reference.

4. Validation of the model

In this section, the validation of the proposed formulation is carried out. To do this, four studies are presented, comparing, in general, results from the literature obtained with the embedded crack model (see Sect. 2) and with the proposed model (see Sect. 3). In all cases, the same meshes used to obtain the results of reference have been employed in order to have a reliable comparison.

In all the diagrams the results obtained with the embedded crack formulation of Sect. 2 are depicted in blue, the results obtained with the proposed smeared crack formulation are depicted in red and in those cases where the numerical diagrams are compared with experimental results, the experimental envelope is depicted in gray.

4.1. Mode I fracture with different fibre proportions

In [20], four mixes of polyolefin fibre-reinforced concrete are studied and their fracture behaviour numerically modeled. Numerical models reproduce three-point bending tests on notched specimens and the concrete dosage is the same in all four mixes, but the fibre proportion varies ranging from 3 kg/m^3 to 10 kg/m^3. Numerical simulations are carried out using the embedded crack formulation (see Sect. 2) and the proposed smeared crack formulation proposed in Sect. 3 with the fracture parameters shown in Tab. 1. Each mix is identified by PFRC (acronym for polyolefin fibre reinforced concrete) and a number that indicates the fibre proportion added in each case. Results correspond to specimens with dimensions 430×100×100 mm^3 (Fig. 5 shows the main dimensions of the model and the boundary conditions). Finite element meshes are composed by constant stress triangular elements, which is required by the embedded crack formulation, and have elements of average size between 4 mm and 4.5 mm.

Table 1: Parameters of the numerical models for PFRC mixes with different fibre proportions.

	E (MPa)	f_t (MPa)	f_k (MPa)	f_r (MPa)	w_k (mm)	w_r (mm)	w_f (mm)
PFRC-3	30000	3.48	0.14	0.28	0.12	2.25	7.5
PFRC-4.5	30000	3.48	0.28	0.68	0.09	2.25	7.5
PFRC-6	30000	3.48	0.43	1.20	0.08	2.25	7.5
PFRC-10	30000	3.48	0.57	1.45	0.07	2.25	7.5

Results for all four mixes are presented in Fig. 6. In all cases, the numerical simulations show a very similar performance when compared with those obtained using the embedded crack formulation. Nevertheless, two main differences can be observed: 1) the numerical results obtained with the smeared crack model show a higher peak load value between 6000 N and 7000 N, which exceeds predictions obtained with the embedded crack formulation and 2) the behaviour after the local maximum that takes place at a deflection of around 3 to 4 mm shows a faster load decay in the case of the smeared crack formulation. Since the parameters of each model (Tab. 1) have been calibrated using the embedded crack formulation, it is expected to obtain a better fit with this formulation, nevertheless, the results obtained with the smeared crack formulation only present one important difference with respect to the experimental results, which corresponds to the excessive initial load peak, which could be easily corrected by adjusting the f_t parameter.

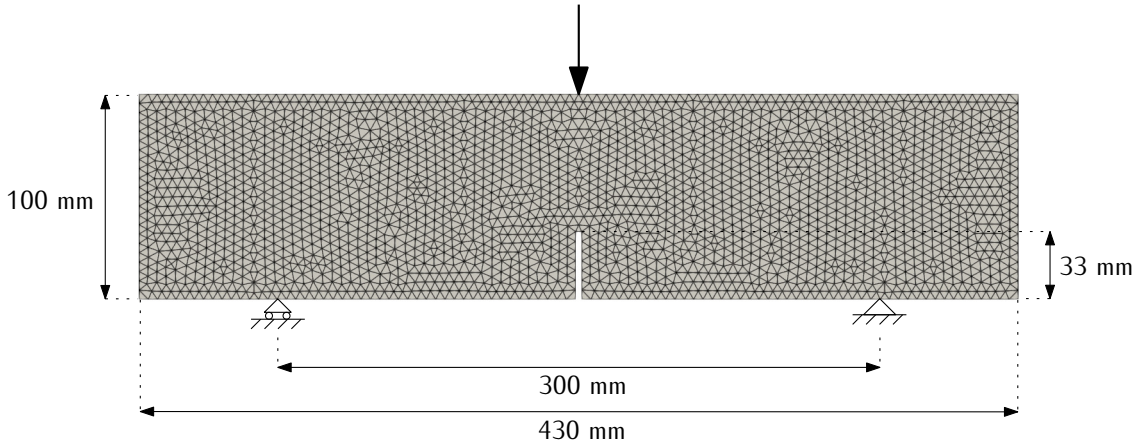

Figure 5: Mesh and boundary conditions used in the simulations of the sutdy of mode I fracture with different fibre proportions.

4.2. Study on mesh refinement

In order to study how mesh refinement may affect the results obtained with the smeared crack model proposed in this work, the same simulation has been carried out using three meshes. The simulation reproduces the results obtained with the small size specimen of [29].

Tab. 2 shows the fracture parameters used in the model and Fig. 7 shows the meshes and the specimen dimensions. All meshes are composed by standard quadrilateral elements with four integration points, remain coarse outside the central region and are refined along the vertical crack path with element sizes of 1, 2 and 3 mm. The overall geometry of the model is the same in all cases, except for the crack width, which is slightly adjusted in each case in order to define square elements along the vertical crack path.

The load-displacement diagrams obtained with these simulation are presented in Fig. 8, where each model is identified with different line styles. The diagrams differ very little no matter the mesh size and even in the detail view shown in Fig. 8b), the peak load at the onset of fracture and the minimum that takes place at a displacement of about 0.4 mm is almost the same for all three cases.

4.3. Analysis of the size effect

Embedded crack model, which inspires the proposed formulation in this work, proves to correctly capture the fracture behaviour of the material with different specimen sizes in [29]. The same models used in that

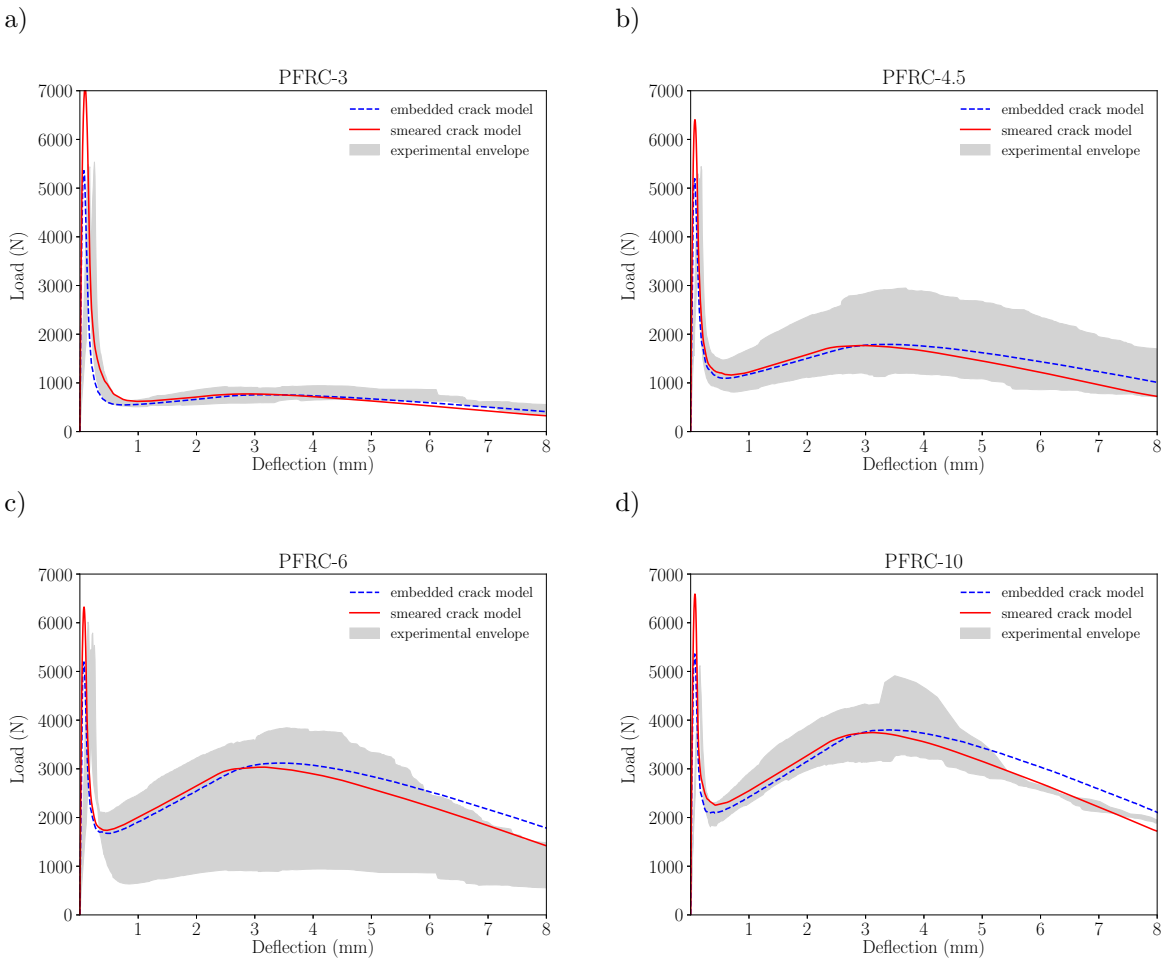

Figure 6: Comparison of the numerical results obtained with both models for a) PFRC-3, b) PFRC-4.5, c) PFRC-6 and d) PFRC-10.

Table 2: Parameters of the numerical models used in the study on mesh refinement.

E (MPa)	f_t (MPa)	f_k (MPa)	f_r (MPa)	w_k (mm)	w_r (mm)	w_f (mm)
22569	3.20	0.57	1.20	0.07	1.65	6.0

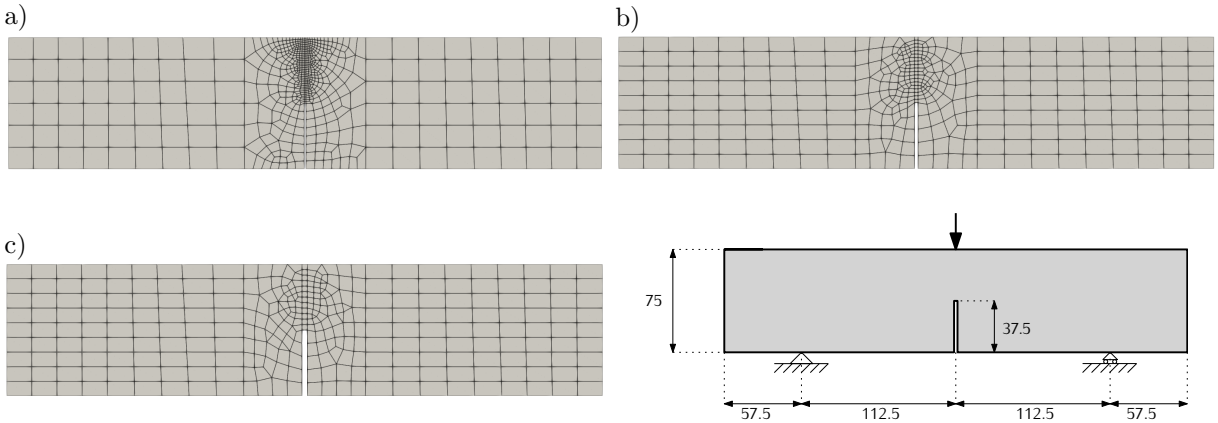

Figure 7: Meshes used in the study on mesh refinement. Element size in the fracture path: a) 1 mm, b) 2 mm, c) 3 mm.

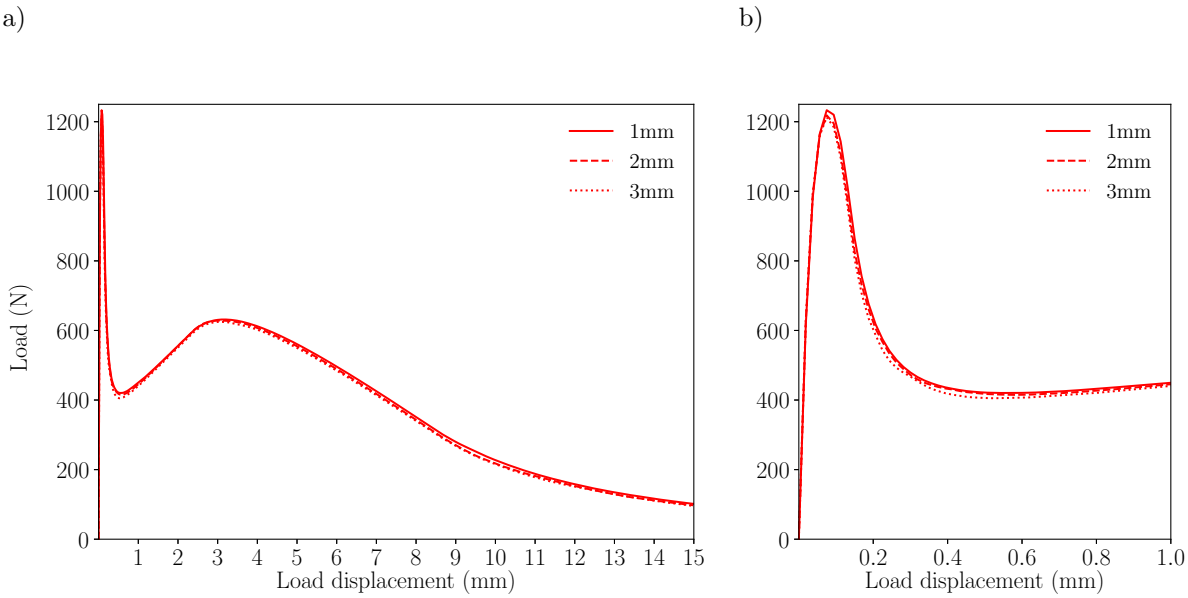

Figure 8: Load-displacement curves obtained with different element sizes of 1, 2 and 3 mm: a) complete diagrams, b) detail of the first part of the diagrams.

reference are here reproduced with the proposed smeared crack formulation and compared with the results shown in [29]. Again, the same finite element meshes are used, as well as the same material parameters, which are presented in Tab. 3. All models have the same meshes as those used in the study of reference and, again, since the embedded model requires the use of constant stress triangular elements, all the elements are triangular and with an only integration point. Meshes are refined along the vertical fracture path and remain coarse out of this region in order to reduce the time of computation. Since the details of these models are the same of those described in [29], the reader can find a more complete description in that reference.

Table 3: Parameters of the numerical models of PFRC-3 specimens of different sizes of reference [29].

	E (MPa)	f_t (MPa)	f_k (MPa)	f_r (MPa)	w_k (mm)	w_r (mm)	w_f (mm)
Small	22569	3.20	0.57	1.20	0.07	1.65	6.0
Medium	22569	3.20	0.57	1.18	0.07	1.65	6.0
Large	22569	3.20	0.57	1.37	0.07	1.65	6.0

Fig. 10 compares the load-displacement diagrams obtained with both formulations for all three specimen sizes. Again, the results obtained with the embedded crack formulation are presented in dashed blue lines while the results obtained with the proposed smeared crack formulation are presented in solid red lines.

The overall behaviour of the smeared crack formulation is similar to the behaviour of the embedded crack formulation, since the local maximum and minimum loads are very similar as well as the shape of the diagrams. The detail view of the diagrams in Fig. 10b) shows that the initial maximum load, which identifies the onset of fracture, is very similar using both formulations and in all three specimen sizes, while the subsequent local minimum, which identifies the load recovery due to the action of fibres crossing the crack, are similar but slightly different depending on the formulation employed, with the embedded crack formulation providing lower values than the smeared crack formulation. In addition to this, in general, the diagrams obtained with the embedded crack formulation after the local maximum that takes place at around a displacement value of 3.5 mm, are horizontally offset if compared with those obtained with the smeared crack formulation. This difference is more noticeable in larger sizes, but it must be noted that this difference is fundamentally a consequence of the previous observation, since it is related to the fact that the local minimum after the peak load, which takes place at around a displacement of 0.5 in these models when the smeared crack formulation is used, is reached at higher displacement values and at lower load values, which

clearly affects the rest of the diagram.

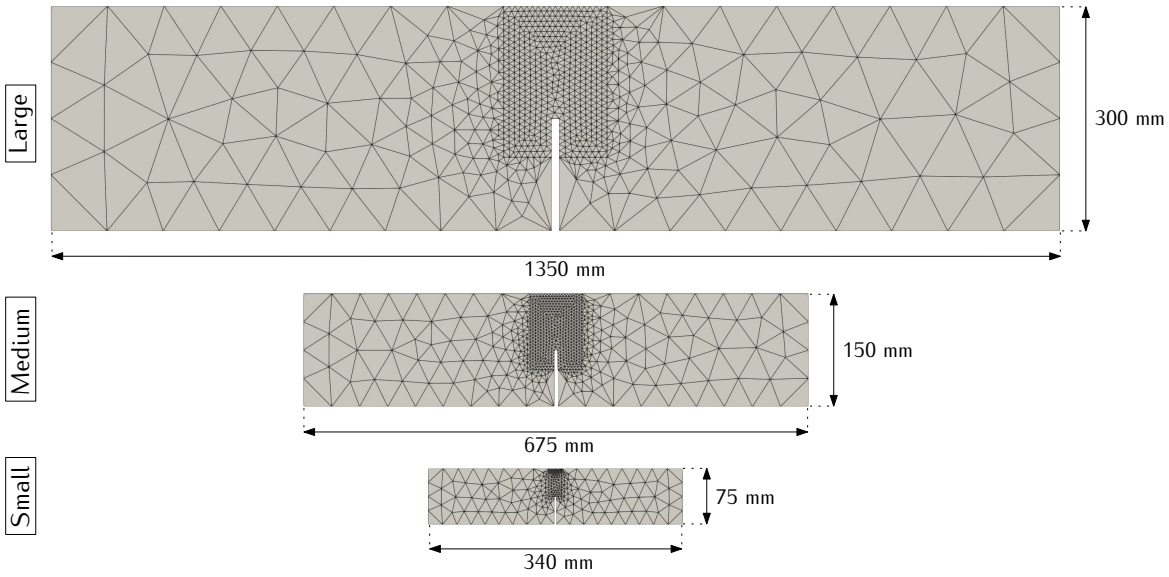

Figure 9: Meshes used in the analysis of the size effect.

a) b)

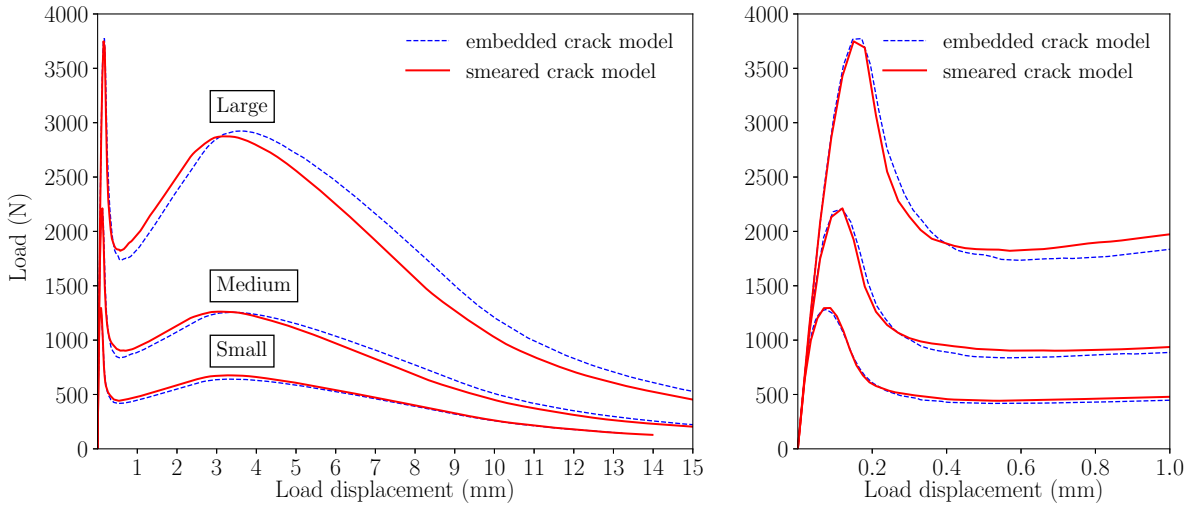

Figure 10: Comparison of the numerical results obtained with both models for different size specimens with PFRC3.

4.4. Fracture under mixed-mode conditions (I+II)

The use of a cohesive crack formulation with a trilinear diagram to reproduce fracture of FRC under a combination of Mode I and Mode II conditions was carried out in [21], where the embedded crack formulation described in Sect. 2 was employed with good results. In the mentioned work, the non-symmetric three-point bending tests proposed in [30] was used, which consists of a variation of the standard three point bending test on notched specimens recommended by RILEM [31], where supports and loading are displaced as shown in Fig. 11. The use of the embedded crack formulation provided good results in several cases, including different fibre proportions and different specimen sizes.

Here, only the results corresponding to different fibre proportions are used for comparison, which correspond to FRC mixes with 3, 6 and 10 kg/m^3 of polyolefin fibres, identified as FC-3, FC-6 and FC-10; the material parameters that define the trilinear diagram in each case are shown in Tab. 4. Regarding the dimensions of the specimens, these results correspond to the geometry shown in Fig. 11 with a height of $D = 150$ mm.

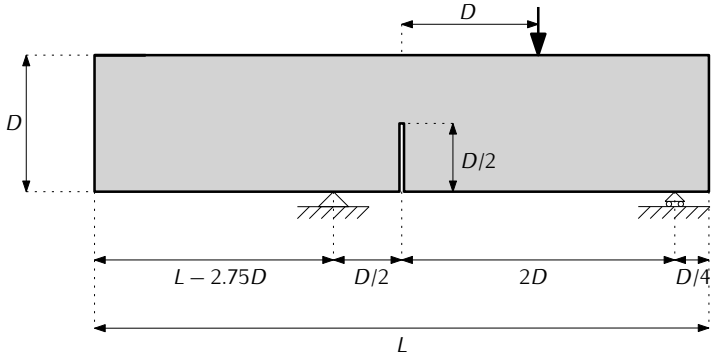

Figure 11: Geometry and boundary conditions used in the study of fracture under mixed-mode conditions (I+II).

Table 4: Parameters of the trilinear diagrams used to reproduce the experimental values on specimens subjected to mixed-loading in [21].

	E (MPa)	f_t (MPa)	f_k (MPa)	f_r (MPa)	w_k (mm)	w_r (mm)	w_f (mm)
FC-3	22569	2.50	0.12	0.25	0.15	2.25	7.5
FC-6	22569	2.50	0.33	0.70	0.14	2.25	7.5
FC-10	22569	2.50	0.75	1.70	0.13	2.25	7.5

Fig. 12 shows the load-displacement diagrams obtained with both models, the representation criteria is the same as used in previous figures, thus the diagrams obtained with the embedded crack formulation are presented in dashed blue lines while the diagrams obtained with the smeared crack formulation are presented with solid red lines; gray shades represent the experimental envelopes. As in the case of the analysis of the size effect in Sect. 4.3, the peak load is slightly higher with the smeared crack formulation, as well as the subsequent local minimum that takes place, in this case, at a load displacement value of around 0.4 mm. In all cases, the load-displacement diagrams remain inside the experimental envelope and do not show big differences when compared with the diagrams obtained with the embedded crack formulation.

It is also interesting to observe that the diagrams obtained with the embedded crack formulation stop at certain load displacement values (≈ 2.7 mm in the case of FC-10,≈ 3.3 in the case of FC-6 and ≈ 2.3 mm in the case of FC-3), while those obtained with the proposed smeared crack formulation extend over 4 mm. This is because the embedded crack model sometimes present convergence problems, that have not been experienced using the proposed smeared crack formulation, which suggests that the latter is more robust than the former.

5. Conclusions

In this work an alternative formulation has been proposed for modeling fracture of fibre reinforced concrete. This formulation is inspired by the embedded crack model used by Alberti et al., which adapted an embedded cohesive crack formulation designed for concrete by using a trilinear softening diagram, which allows reproducing fracture behaviour of FRC.

The model proposed in this work corresponds to a smeared crack formulation where the cracking process is driven by a scalar damage variable ranging from 0 (undamaged) to 1 (totally damaged). The formulation presented here has been derived to use the same input parameters employed in the embedded crack model

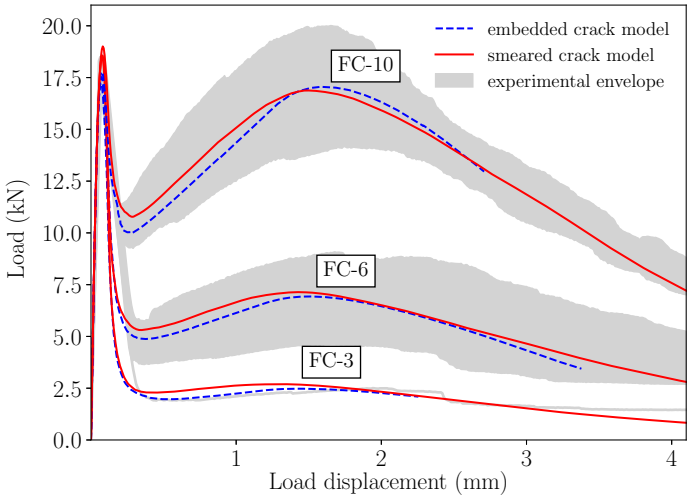

Figure 12: Comparison of the numerical results obtained with both models on FRC specimens subjected to mixed loading. Shaded areas represent the experimental envelopes obtained in [21].

that is used as reference in order to allow a reliable comparison of both formulations. Therefore, the proposed formulation has been validated by comparing its behaviour with the embedded crack formulation of reference. The same meshes and material parameters have been used in each case and the following conclusions can be drawn from the results presented here:

- The proposed smeared crack formulation produces very similar results for different proportions of fibre addition when compared with those provided by the embedded crack formulation. Slight differences have been found, but the overall behaviour of the fracture process is remarkably similar.
- When this formulation is used with different size meshes (element sizes of 1, 2 and 3 mm have been compared), the resulting load-displacement diagrams are almost coincident in all three analysed cases.
- As in the case of the embedded crack formulation, the proposed smeared crack model captures the size effect of fracture in FRC and is able to reproduce fracture under mode I and under a combination of modes I and II.

In addition to these conclusions, the proposed formulation has some advantages over the embedded crack formulation in which it is inspired:

- Cracking is not limited to only three directions, as in the embedded crack formulation, thus it can develop at any direction on the plane.
- This formulation can be used with any bidimensional finite element, and is not limited to triangular elements, which can lead to some numerical problems.
- This formulation can be used on finite elements with more than one integration point.
- The formulation proposed in this work is implemented in OOFEM, a free finite element code available to any interested in studying fracture of FRC.
- The behaviour of the new formulation is similar to that of the formulation of reference, which makes all the knowledge acquired with the former model valid with the new one.

Acknowledgements

The author wishes to express his gratitude to Prof. Enfedaque, who has kindly provided the meshes, the material parameters and the load-displacement diagrams of the models computed with the embedded crack formulation of Sect. 4.1.

References

[1] Sweden Standard SS812310: 2014. Svenska Institutet för Standarder (SIS)—Bygg och anläggning: Stockholm, Sweden; 2014.

[2] Código estructural: Anejos 1-18. Ministerio de Transportes, Movilidad y Agenda Urbana, Madrid, España; 2021.

[3] fib Model Code 2010. Fédération Internationale du Béton fib/International Federation for Structural Concrete: Paris, France. Ernst & Sohn, Wiley; 2013.

[4] China CECS38:2004. Technical Specification for Fiber Reinforced Concrete Structures provides Guidelines for Various Applications. Dalian University of Technology: Dalian, China; 2004.

[5] Cánovas MF. Hormigones reforzados con fibras de acero. Informes de la Construcción. 1982;34(342):5–17.

[6] Zollo RF. Fiber-reinforced concrete: an overview after 30 years of development. Cement and Concrete Composites. 1997;19(2):107–122. Available from: https://www.sciencedirect.com/science/article/pii/S0958946596000467.

[7] Wang Y, Yang D, Zhou M. The present research condition and trend of polypropylene fiber concrete. Concrete. 2004;1:24–26.

[8] Das CS, Dey T, Dandapat R, Mukharjee BB, Kumar J. Performance evaluation of polypropylene fibre reinforced recycled aggregate concrete. Construction and Building Materials. 2018;189:649–659.

[9] Correia JR, Ferreira J, Branco FA. A rehabilitation study of sandwich GRC facade panels. Construction and Building Materials. 2006;20(8):554–561. Available from: https://www.sciencedirect.com/science/article/pii/S095006180500084X.

[10] Enfedaque A, Cendón D, Gálvez F, Sánchez-Gálvez V. Failure and impact behavior of facade panels made of glass fiber reinforced cement(GRC). Engineering Failure Analysis. 2011;18(7):1652–1663. The Fourth International Conference on Engineering Failure Analysis Part 2. Available from: https://www.sciencedirect.com/science/article/pii/S1350630711000112.

[11] Ferreira J, Branco F. Structural application of GRC in telecommunication towers. Construction and building materials. 2007;21(1):19–28.

[12] Serna P, Arango S, Ribeiro T, Núñez A, Garcia-Taengua E. Structural cast-in-place SFRC: technology, control criteria and recent applications in Spain. Materials and structures. 2009;42(9):1233–1246.

[13] Alberti M, Enfedaque A, Gálvez J. Fracture mechanics of polyolefin fibre reinforced concrete: Study of the influence of the concrete properties, casting procedures, the fibre length and specimen size. Engineering Fracture Mechanics. 2016;154:225–244.

[14] Cervenka J. Discrete crack modeling in concrete structures. University of Colorado at Boulder; 1994.

[15] Jirásek M. Damage and smeared crack models. In: Numerical modeling of concrete cracking. Springer; 2011. p. 1–49.

[16] Jirásek M, Zimmermann T. Embedded crack model: I. Basic formulation. International journal for numerical methods in engineering. 2001;50(6):1269–1290.

[17] Jirásek M, Zimmermann T. Embedded crack model. Part II: Combination with smeared cracks. International Journal for Numerical Methods in Engineering. 2001;50(6):1291–1305.

[18] Hillerborg A, Modéer M, Petersson PE. Analysis of crack formation and crack growth in concrete by means of fracture mechanics and finite elements. *Cem Concr Res*. 1976;6(6):773 – 781.

[19] Havlásek P, Kabele P. A detailed description of the computer implementation of SHCC material model in OOFEM. CTU in Prague. 2017;.

[20] Alberti M, Enfedaque A, Gálvez J, Reyes E. Numerical modelling of the fracture of polyolefin fibre reinforced concrete by using a cohesive fracture approach. Composites Part B: Engineering. 2017;111:200–210.

[21] Suárez F, Gálvez J, Enfedaque A, Alberti M. Modelling fracture on polyolefin fibre reinforced concrete specimens subjected to mixed-mode loading. Engineering Fracture Mechanics. 2019;211:244–253.

[22] Jirásek M, Bauer M. Numerical aspects of the crack band approach. Computers & structures. 2012;110:60–78.

[23] Oliver J. A consistent characteristic length for smeared cracking models. International Journal for Numerical Methods in Engineering. 1989;28(2):461–474.

[24] Patzák B. OOFEM—an object-oriented simulation tool for advanced modeling of materials and structures. Acta Polytechnica. 2012;52(6).

[25] Sancho JM, Planas J, Cendón DA, Reyes E, Gálvez JC. An embedded crack model for finite element analysis of concrete fracture. Engineering Fracture Mechanics. 2007;74(1):75 – 86. Fracture of Concrete Materials and Structures. Available from: `http://www.sciencedirect.com/science/article/pii/S0013794406000488`.

[26] Reyes E, Gálvez JC, Casati MJ, Cendón DA, Sancho JM, Planas J. An embedded cohesive crack model for finite element analysis of brickwork masonry fracture. Engineering Fracture Mechanics. 2009;76(12):1930 – 1944. Available from: `http://www.sciencedirect.com/science/article/pii/S0013794409001490`.

[27] Bažant ZP, Planas J. *Fracture and size effect in concrete and other quasibrittle materials*. CRC press; 1997.

[28] Bažant ZP, Oh BH. Crack band theory for fracture of concrete. Matériaux et construction. 1983;16(3):155–177.

[29] Suárez F, Gálvez JC, Alberti MG, Enfedaque A. Fracture and Size Effect of PFRC Specimens Simulated by Using a Trilinear Softening Diagram: A Predictive Approach. Materials. 2021;14(14). Available from: `https://www.mdpi.com/1996-1944/14/14/3795`.

[30] Gálvez JC, Elices M, Guinea G, Planas J. Mixed mode fracture of concrete under proportional and nonproportional loading. *Int J Fract*. 1998;94(3):267–284.

[31] RILEM. Determination of the Fracture Energy of Mortar and Concrete by Means of Three-Point Bend Tests on Notched Beams. *Mater Struct*. 1985;18(106):285–290.